A Letters Journal Exploring the Frontiers of Physics

May 2020

EPL, **130** (2020) 34001 www.epljournal.org
doi: 10.1209/0295-5075/130/34001

Nonlinear thermal conductivities of core-shell metamaterials: Rigorous theory and intelligent application

C. Su, L. J. Xu[a] and J. P. Huang[b]

Department of Physics, State Key Laboratory of Surface Physics, and Key Laboratory of Micro and Nano Photonic Structures (MOE), Fudan University - Shanghai 200438, China

received 3 March 2020; accepted in final form 13 May 2020
published online 29 May 2020

PACS 44.10.+i – Heat conduction
PACS 05.70.-a – Thermodynamics
PACS 81.05.Zx – New materials: theory, design, and fabrication

Abstract – Nonlinear (temperature-dependent) thermal conductivities are common in nature, so their in-depth studies are valuable to practical applications. However, for core-shell metamaterials with nonlinear thermal conductivities, only an approximate theory was proposed to deal with weak nonlinearity, and almost no theory can handle strong nonlinearity strictly. To solve this problem, we propose a rigorous theory under certain conditions to calculate the effective thermal conductivities of core-shell metamaterials with nonlinear thermal conductivities, whether weak or strong. Furthermore, we design intelligent applications with the present theory. We take thermal radiation with the Rosseland diffusion approximation as an example, which is a typical system containing nonlinear thermal conductivities, and further realize switchable functions between concentrating and cloaking. The present theory and application are confirmed by finite-element simulations. Our results lay the theoretical foundation for nonlinear core-shell metamaterials and provide insights into nonlinear thermal management.

Copyright © EPLA, 2020

Introduction. – Thermal energy is of particular significance to human beings, so researchers have paid lasting attention to the key parameter for manipulating thermal energy, say, thermal conductivities. Since the proposal of transformation thermotics [1,2], thermal metamaterials with linear thermal conductivities have been designed intensively, having cloaking [3–12], concentrating [3,8, 12–14], rotating [3,11,12], camouflaging [7,15–27], and chameleon-like behaviors [28–30]. Here, "linear" means that thermal conductivities are temperature-independent.

Thermal metamaterials with nonlinear (temperature-dependent) thermal conductivities have also attracted research interest. For example, nonlinear transformation thermotics was proposed to design macroscopic thermal diodes [31,32]; the effective nonlinear thermal conductivities of periodic structures were calculated [33,34]; an approximate theory was put forward to handle core-shell metamaterials with weak nonlinearity [35]; and nonlinear thermal conductivities were also used to design practical applications [36–42]. Here, "weak nonlinearity" means that linear (temperature-independent) terms are the dominant ones of nonlinear thermal conductivities.

However, most theories are approximate and applicable for only weak nonlinearity, which limits practical applications. To solve this problem, we study core-shell metamaterials with nonlinear thermal conductivities, whether weak or strong. With the only assumption that the ratio of the nonlinear thermal conductivities of the core and shell is a constant, we establish a rigorous theory to calculate their effective thermal conductivity. Certainly, the rigorous theory can also be extended to more general cases with a small cost of accuracy.

With the present theory, we are allowed to design intelligent applications by taking advantage of nonlinear thermal conductivities. We take thermal radiation with the Rosseland diffusion approximation as an example, which is a typical system containing nonlinear thermal conductivities [43,44]. We further design a switchable device which can achieve thermal concentrating at low temperatures and thermal cloaking at high temperatures. Such a design is for a practical reason: we expect to harvest

[a] E-mail: 13307110076@fudan.edu.cn
[b] E-mail: jphuang@fudan.edu.cn

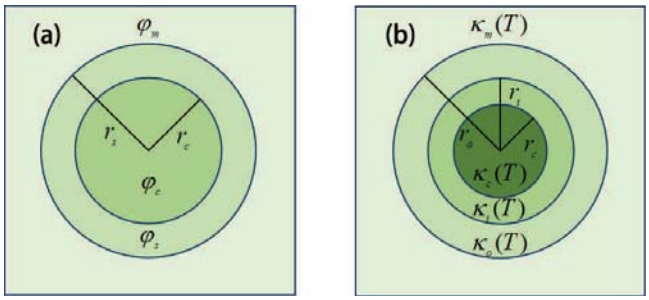

Fig. 1: Schematic diagrams of (a) a core-shell metamaterial and (b) a core-shell-shell (bilayer) metamaterial embedded in the matrix.

thermal energy at low temperatures thus requiring a concentrator, whereas large heat fluxes (resulting from high temperatures) may damage the apparatus thus requiring a cloak. We perform finite-element simulations to confirm the design, and the results agree well with the theory.

Two-dimensional theory. – We consider a core-shell metamaterial embedded in a matrix (see fig. 1(a)). The nonlinear thermal conductivities of the core $\kappa_c(T)$, shell $\kappa_s(T)$, and matrix $\kappa_m(T)$ are denoted as

$$\kappa_c(T) = \sum_{i=1}^{n} \alpha_i T^{\lambda_i}, \tag{1}$$

$$\kappa_s(T) = \sum_{i=1}^{n} \beta_i T^{\lambda_i}, \tag{2}$$

$$\kappa_m(T) = \sum_{i=1}^{n} \gamma_i T^{\lambda_i}, \tag{3}$$

where α_i, β_i, γ_i, and λ_i can be any constants. Equations (1), (2), or (3) are the most common form of nonlinear thermal conductivities. To establish a rigorous theory for nonlinear thermal conductivities, we firstly consider a special case with $\kappa_s(T)/\kappa_c(T) = \mu$ and $\kappa_m(T)/\kappa_c(T) = \nu$, thus yielding $\beta_i/\alpha_i = \mu$ and $\gamma_i/\alpha_i = \nu$, where μ and ν are two constants. A passive and steady process of thermal conduction satisfies the Laplace equation $\boldsymbol{\nabla} \cdot [-\kappa(T)\boldsymbol{\nabla} T] = 0$. Therefore, the dominant equation in the core can be expressed as

$$\boldsymbol{\nabla} \cdot [-\kappa_c(T)\boldsymbol{\nabla} T] = \boldsymbol{\nabla} \cdot \left[-\sum_{i=1}^{n} \alpha_i T^{\lambda_i} \boldsymbol{\nabla} T \right] = 0. \tag{4}$$

By setting $\alpha_j/\alpha_i = \omega_j$, we can obtain

$$\boldsymbol{\nabla} \cdot \left[-\alpha_i \boldsymbol{\nabla} \left(\sum_{j=1}^{n} \frac{\omega_j}{\lambda_j + 1} T^{\lambda_j + 1} \right) \right] = 0. \tag{5}$$

With $\beta_i/\alpha_i = \mu$, $\gamma_i/\alpha_i = \nu$, and $\alpha_j/\alpha_i = \omega_j$, we can also derive $\beta_j/\beta_i = \omega_j$ and $\gamma_j/\gamma_i = \omega_j$, so the dominant equation in the shell and matrix can be expressed as

$$\boldsymbol{\nabla} \cdot \left[-\beta_i \boldsymbol{\nabla} \left(\sum_{j=1}^{n} \frac{\omega_j}{\lambda_j + 1} T^{\lambda_j + 1} \right) \right] = 0, \tag{6}$$

$$\boldsymbol{\nabla} \cdot \left[-\gamma_i \boldsymbol{\nabla} \left(\sum_{j=1}^{n} \frac{\omega_j}{\lambda_j + 1} T^{\lambda_j + 1} \right) \right] = 0. \tag{7}$$

We make a substitution

$$\varphi = \sum_{j=1}^{n} \frac{\omega_j}{\lambda_j + 1} T^{\lambda_j + 1}, \tag{8}$$

so eqs. (5)–(7) can be expressed in cylindrical coordinates (r, θ) as

$$\frac{\partial}{\partial r}\left(r \frac{\partial \varphi}{\partial r} \right) + \frac{\partial}{\partial \theta}\left(\frac{\partial \varphi}{r \partial \theta} \right) = 0. \tag{9}$$

Equation (9) is a linear equation, so its general solution is [45]

$$\varphi = A_0 + B_0 \ln r + \sum_{i=1}^{\infty} [A_i \cos(i\theta) + B_i \sin(i\theta)] r^i + \sum_{j=1}^{\infty} [C_j \cos(j\theta) + D_j \sin(j\theta)] r^{-j}. \tag{10}$$

As is shown in fig. 1(a), we suppose that the core, shell, and matrix have φ_c, φ_s, and φ_m, respectively. The associated boundary conditions can be expressed as

$$\begin{cases} T_c|_{r=r_c} = T_s|_{r=r_c}, \\ T_s|_{r=r_s} = T_m|_{r=r_s}, \\ -\kappa_c(\partial T_c/\partial r)|_{r=r_c} = -\kappa_s(\partial T_s/\partial r)|_{r=r_c}, \\ -\kappa_s(\partial T_s/\partial r)|_{r=r_s} = -\kappa_m(\partial T_m/\partial r)|_{r=r_s}, \end{cases} \tag{11}$$

where r_c and r_s are the radii of the core and shell, respectively. Equation (11) indicates the temperature continuity and the normal heat flux continuity. With eqs. (8) and (11), we can rewrite down the boundary conditions as

$$\begin{cases} \varphi_c|_{r\to 0} \text{ is finite}, \\ \varphi_c|_{r=r_c} = \varphi_s|_{r=r_c}, \\ \varphi_s|_{r=r_s} = \varphi_m|_{r=r_s}, \\ -\alpha_i(\partial \varphi_c/\partial r)|_{r=r_c} = -\beta_i(\partial \varphi_s/\partial r)|_{r=r_c}, \\ -\beta_i(\partial \varphi_s/\partial r)|_{r=r_s} = -\gamma_i(\partial \varphi_m/\partial r)|_{r=r_s}, \\ \varphi_m|_{r\to\infty} = -|\boldsymbol{\nabla}\varphi_0| r \cos\theta, \end{cases} \tag{12}$$

where $|\boldsymbol{\nabla}\varphi_0|$ is the modulus of the uniform thermal field. With the symmetry requirement of boundary conditions, we can know $\varphi_c = A_{c1} r \cos\theta$, $\varphi_s = (A_{s1} r + C_{s1} r^{-1}) \cos\theta$, and $\varphi_m = (A_{m1} r + C_{m1} r^{-1}) \cos\theta$. When the nonlinear thermal conductivity of the matrix is equal to the effective thermal conductivity of the core-shell metamaterial, the

isotherms in the matrix are parallel lines which requires $C_{m1} = 0$. Therefore, by solving eq. (12) with $C_{m1} = 0$, we can obtain

$$\gamma_i = \beta_i \frac{\alpha_i + \beta_i + (\alpha_i - \beta_i)p}{\alpha_i + \beta_i - (\alpha_i - \beta_i)p}, \tag{13}$$

where $p = r_c^2/r_s^2$ is the core fraction. Since we do not restrict the value of i, it can take values from 1 to n. Therefore, the nonlinear thermal conductivity of the matrix (say, the effective thermal conductivity of the core-shell metamaterial) should satisfy

$$\kappa_m(T) = \sum_{i=1}^{n} \beta_i \frac{\alpha_i + \beta_i + (\alpha_i - \beta_i)p}{\alpha_i + \beta_i - (\alpha_i - \beta_i)p} T^{\lambda_i}. \tag{14}$$

Two-dimensional simulations. – To confirm our theory, we put a core-shell metamaterial in a matrix, and set the thermal conductivity of the matrix to be the same as the effective thermal conductivity of the core-shell metamaterial, as required by eq. (14). The left and right sides are fixed at 300 K and 900 K, respectively. The upper and lower sides are thermally insulated. Then, we compare the temperature distributions in the matrix with a finite-element method (based on the "solid heat transfer" module of COMSOL MULTIPHYSICS [46]) and an analytical method.

Firstly, we perform a finite-element simulation to obtain the temperature distribution of the system (see fig. 2(a)). We also plot the $\partial T/\partial y$ distribution in the matrix (see fig. 2(b)). For quantitative comparisons, we perform finite-element simulations with different temperature intervals, and export the temperature distributions on the dashed line in fig. 2(a) (see the lines in fig. 2(c)). We also perform finite-element simulations with different core fractions, and export the $\partial T/\partial y$ distribution on the dashed line in fig. 2(b) (fig. 2(d)). The values of $\partial T/\partial y$ are always zero, indicating that the core-shell structure does not distort the temperature distribution in the matrix.

Secondly, we calculate the temperature distributions with an analytical method. For this purpose, we denote the temperatures of left and right sides as T_l and T_r, respectively. With the substitution of eq. (8), T_l and T_r become φ_l and φ_r, respectively. Therefore, we can obtain $\varphi_m = (\varphi_r - \varphi_l)x/W + (\varphi_r + \varphi_l)/2$, where W is the width of the system. Then, the temperature values can be derived by solving eq. (8). These analytical values are also plotted by symbols in fig. 2(c), which are consistent with the simulation values. Therefore, the present theory is rigorous.

We have established a rigorous theoretical framework for calculating the effective thermal conductivities of core-shell metamaterials with nonlinear thermal conductivities, whether weak or strong. As mentioned above, our theory is rigorous under the conditions of $\kappa_s(T)/\kappa_c(T) = \mu$ and $\kappa_m(T)/\kappa_c(T) = \nu$. We should point out that the theory is also applicable when these two conditions are not

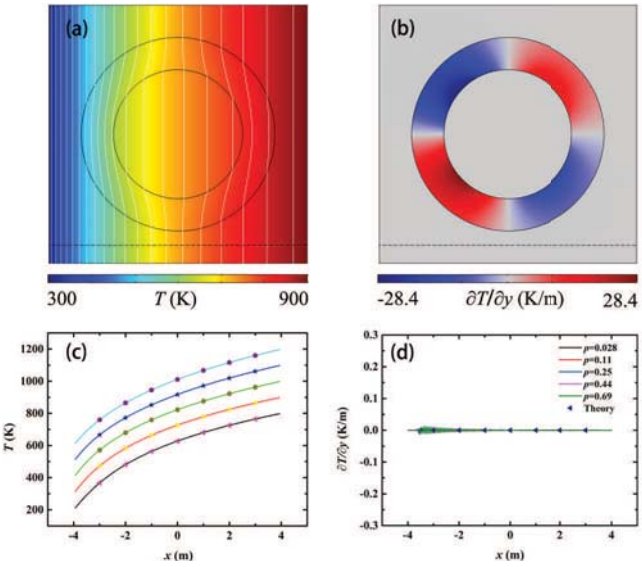

Fig. 2: Two-dimensional simulations of a rigorous case. The simulation size is $8 \times 8\,\mathrm{m}^2$, $r_c = 2\,\mathrm{m}$, and $r_s = 3\,\mathrm{m}$ ($p = 0.44$). The nonlinear thermal conductivities of the core, shell, and matrix are $10^2 + 10^{-2}T + 10^{-4}T^2 + 10^{-6}T^3\,\mathrm{W/(m \cdot K)}$, $50+5\times10^{-3}T+5\times10^{-5}T^2+5\times10^{-7}T^3\,\mathrm{W/(m \cdot K)}$, and $67.39+6.739 \times 10^{-3}T + 6.739 \times 10^{-5}T^2 + 6.739 \times 10^{-7}T^3\,\mathrm{W/(m \cdot K)}$, respectively. (a) Temperature distribution of the system. (b) $\partial T/\partial y$ distribution of the system. (c) Temperature distributions on the dashed line in (a) with different temperature intervals. (d) $\partial T/\partial y$ distribution on the dashed line in (b) with different core fractions.

met. In fact, if these two conditions are not met, the effective thermal conductivities of core-shell metamaterials are not well defined because the isotherms in the matrix can never be parallel lines. Therefore, we should define a physical quantity to test the performance of the theory. Since the value of $\partial T/\partial y$ can reflect the distortion degree of isotherms, we use the average value of $|\partial T/\partial y|$ in the matrix (denoted as ξ) to test the theory, namely

$$\xi = \frac{\int_\Omega |\partial T/\partial y| \mathrm{d}x\mathrm{d}y}{\int_\Omega \mathrm{d}x\mathrm{d}y}, \tag{15}$$

where Ω denotes the integration area, namely the matrix. When $\xi = 0$, the isotherms are strictly parallel lines, indicating a rigorous case. The smaller the value of ξ is, the better the approximation is.

To confirm the statement, we keep $\kappa_c(T)$ unchanged, and set $\kappa_s(T)$ to be the same as $\kappa_c(T)$ except for one nonlinear term. $\kappa_m(T)$ is still calculated by eq. (14). We perform finite-element simulations with different values of $\kappa_s(T)$, and the results are presented in figs. 3(a)–(e) with the same temperature interval, say, 300–900 K. To test the distortion degree of isotherms in figs. 3(a)–(e), we also export the corresponding values of ξ. Meanwhile, we also change the temperature intervals and obtain the values of ξ. These results are presented in fig. 3(f). We can find that ξ is no longer zero, indicating that $\kappa_m(T)$ derived

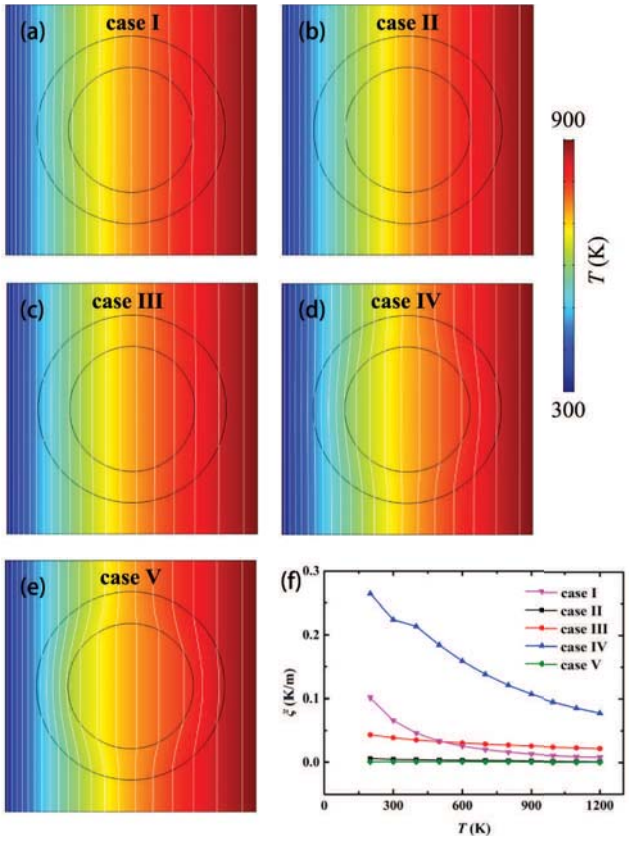

Fig. 3: Two-dimensional simulations of general cases. (a)–(e) Temperature distributions of five different cases with the left and right temperatures kept at 300 K and 900 K, respectively. The thermal conductivity of the core is $10^2 + 10^{-2}T + 10^{-4}T^2 + 10^{-6}T^3\,\mathrm{W/(m\cdot K)}$ for all cases. The thermal conductivity of the shell and matrix are respectively $50 + 10^{-2}T + 10^{-4}T^2 + 10^{-6}T^3\,\mathrm{W/(m\cdot K)}$ and $67.39 + 10^{-2}T + 10^{-4}T^2 + 10^{-6}T^3\,\mathrm{W/(m\cdot K)}$ for case I; $100 + 5\times 10^{-3}T + 10^{-4}T^2 + 10^{-6}T^3\,\mathrm{W/(m\cdot K)}$ and $100 + 6.739\times 10^{-3}T + 10^{-4}T^2 + 10^{-6}T^3\,\mathrm{W/(m\cdot K)}$ for case II; $100 + 10^{-2}T + 5\times 10^{-5}T^2 + 10^{-6}T^3\,\mathrm{W/(m\cdot K)}$ and $100 + 10^{-2}T + 6.739\times 10^{-5}T^2 + 10^{-6}T^3\,\mathrm{W/(m\cdot K)}$ for case III; $100 + 10^{-2}T + 10^{-4}T^2 + 5\times 10^{-7}T^3\,\mathrm{W/(m\cdot K)}$ and $100 + 10^{-2}T + 10^{-4}T^2 + 6.739\times 10^{-7}T^3\,\mathrm{W/(m\cdot K)}$ for case IV; and $50 + 5\times 10^{-3}T + 5\times 10^{-5}T^2 + 5\times 10^{-7}T^3\,\mathrm{W/(m\cdot K)}$ and $67.39 + 6.739\times 10^{-3}T + 6.739\times 10^{-5}T^2 + 6.739\times 10^{-7}T^3\,\mathrm{W/(m\cdot K)}$ for case V. (f) ξ-T profile where T represents the temperature of the left side. The temperatures of left and right sides change, but the temperature difference is kept at 600 K.

from eq. (14) is not exactly the effective thermal conductivity of the core-shell metamaterial. However, the values of ξ are no more than 0.2643 in the simulations, indicating that the isotherms are distorted slightly and $\kappa_m(T)$ is still close to the effective thermal conductivity of the core-shell metamaterial.

Intelligent applications. – Nonlinear thermal conductivities are common in nature, For instance, the thermal conductivities of some glass are measured to be proportional to $T^{1.8}$ in low temperatures [47], and the thermal conductivities of high purity crystals of silicon and germanium decrease faster than T^{-1} from 3 K to their melting point [48]. Here we take thermal radiation as an example. With the Rosseland diffusion approximation, thermal radiation is of T^3 temperature-dependence [43,44], which belongs to strong nonlinearity. Combining thermal conduction with thermal radiation, a passive and steady process of heat transfer is dominated by

$$\boldsymbol{\nabla}\cdot\boldsymbol{J}_{total} = \boldsymbol{\nabla}\cdot(\boldsymbol{J}_{con} + \boldsymbol{J}_{rad}) = 0. \tag{16}$$

The conductive flux is determined by the Fourier Law $\boldsymbol{J}_{con} = -\kappa\boldsymbol{\nabla}T$, and the radiative flux is given by the Rosseland diffusion approximation $\boldsymbol{J}_{rad} = -\tau T^3\boldsymbol{\nabla}T$. The radiative coefficient takes the value $\tau = 16/3\eta^{-1}n^2\sigma$, where η is the Rosseland mean extinction coefficient, n is the relative refractive index, and $\sigma = 5.67\times 10^{-8}\ \mathrm{W/(m^2\cdot K^4)}$ is the Stefan-Boltzmann constant. Therefore, eq. (16) can be also expressed as

$$\boldsymbol{\nabla}\cdot[-(\kappa + \tau T^3)\boldsymbol{\nabla}T] = 0. \tag{17}$$

Clearly, a thermal conduction-radiation problem can be converted to the problem of nonlinear thermal conductivity with $\kappa(T) = \kappa + \tau T^3$, so the present theory of eq. (14) is still applicable.

For a matrix with a fixed nonlinear thermal conductivity, we hope to design a core-shell-shell (bilayer) metamaterial embedded in the matrix (see fig. 1(b)), which can achieve thermal concentrating at low temperatures and thermal cloaking at high temperatures. To achieve this goal, we denote the nonlinear thermal conductivities of the core $\kappa_c(T)$, inner shell $\kappa_i(T)$, and outer shell $\kappa_o(T)$ as

$$\begin{cases} \kappa_c(T) = \kappa_c + \tau_c T^3, \\ \kappa_i(T) = \kappa_i + \tau_i T^3, \\ \kappa_o(T) = \kappa_o + \tau_o T^3, \end{cases} \tag{18}$$

where κ_c, κ_i, κ_o, τ_c, τ_i, and τ_o are six constants.

For multilayered structures, our theory is still applicable. Firstly, we can calculate the effective thermal conductivity of the core and the first shell $\kappa^{(1)}(T)$. Secondly, we regard the core and the first shell as an equivalent core with thermal conductivity $\kappa^{(1)}(T)$, and calculate the effective thermal conductivity of the equivalent core and the second layer $\kappa^{(2)}(T)$. With successive iterations, we can obtain the effective thermal conductivity of the multilayered structure, namely $\kappa_m(T)$.

At low temperatures, nonlinear thermal conductivities are mainly dominated by linear terms, so the influence of temperature-dependent terms (τ_c, τ_i, and τ_o) can be ignored. To keep the temperature distribution of the matrix unaffected, the thermal conductivity of the matrix should satisfy

$$\begin{cases} \kappa^{(1)}(T) = \kappa_i\dfrac{\kappa_c + \kappa_i + (\kappa_c - \kappa_i)p_1}{\kappa_c + \kappa_i - (\kappa_c - \kappa_i)p_1}, \\ \kappa_m(T) = \kappa_o\dfrac{\kappa^{(1)}(T) + \kappa_o + [\kappa^{(1)}(T) - \kappa_o]p_2}{\kappa^{(1)}(T) + \kappa_o - [\kappa^{(1)}(T) - \kappa_o]p_2}, \end{cases} \tag{19}$$

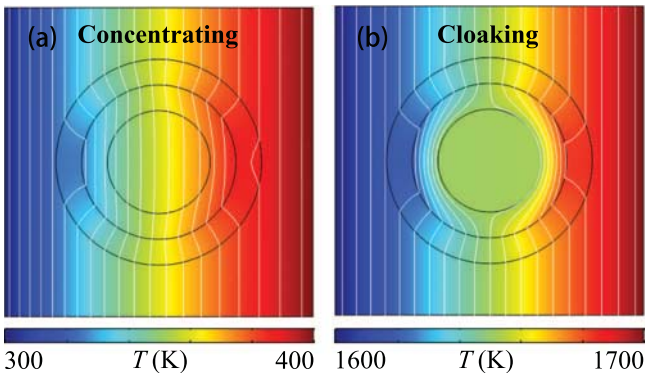

Fig. 4: (a) Thermal concentrating at low temperatures. (b) Thermal cloaking at high temperatures. The thermal conductivities of the core, inner shell, and outer shell are $1.000 + 5.000 \times 10^{-7} T^3\,\mathrm{W/(m \cdot K)}$, $17.00\,\mathrm{W/(m \cdot K)}$, $307.8 + 3.571 \times 10^{-3} T^3\,\mathrm{W/(m \cdot K)}$, respectively. The thermal conductivity of the matrix is set as $200.0 + 1.000 \times 10^{-3} T^3\,\mathrm{W/(m \cdot K)}$.

where $p_1 = r_c^2/r_i^2, p_2 = r_i^2/r_o^2$, and $\kappa^{(1)}(T)$ is the effective thermal conductivity of the core and inner shell. Besides, the thermal conductivity of the core should be smaller than that of the matrix so that the temperature gradient in the core is larger than that in the matrix, ensuring the concentrating effect. Since temperature-dependent terms are ignored at low temperature, eq. (19) is independent of temperature.

At high temperatures, nonlinear thermal conductivities are mainly dominated by the temperature-dependent terms, so the influence of linear terms (κ_c, κ_i, and κ_o) can be ignored. To achieve the purpose of thermal cloaking, the thermal conductivity of the inner shell is set near to zero, namely $\tau_i \approx 0\,\mathrm{W/(m \cdot K)}$. With such a setting, the effective thermal conductivity of the core and inner shell is also near to zero, namely $\kappa^{(1)}(T) \approx 0\,\mathrm{W/(m \cdot K)}$. To make the matrix temperature distribution undistorted by the bilayer structure, the nonlinear thermal conductivity of the matrix should satisfy

$$\begin{cases} \kappa^{(1)}(T) \approx 0, \\ \kappa_m(T) = \tau_o \dfrac{1-p_2}{1+p_2} T^3. \end{cases} \tag{20}$$

Combing eqs. (19) and (20), we can obtain the thermal conductivity of the matrix in both low and high temperatures as

$$\begin{cases} \kappa^{(1)}(T) = \kappa_i \dfrac{\kappa_c + \kappa_i + (\kappa_c - \kappa_i)p_1}{\kappa_c + \kappa_i - (\kappa_c - \kappa_i)p_1}, \\ \kappa_m(T) = \kappa_o \dfrac{\kappa^{(1)}(T) + \kappa_o + [\kappa^{(1)}(T) - \kappa_o]p_2}{\kappa^{(1)}(T) + \kappa_o - [\kappa^{(1)}(T) - \kappa_o]p_2} \\ \qquad\qquad + \tau_o \dfrac{1-p_2}{1+p_2} T^3. \end{cases} \tag{21}$$

We also perform finite-element simulations to confirm the design (see fig. 4). The left and right sides are fixed at constant temperatures. The upper and lower sides are thermally insulated.

Figure 4(a) shows thermal concentrating at low temperatures. The structure has an inner diameter of 1 m, an inner shell thickness of 0.5 m, and an outer shell thickness of 0.5 m, embedded in the matrix with side length of 6 m. Corresponding thermal conductivities are described in the figure caption. The left and right sides are set at 300 K and 400 K, respectively. Color surfaces represent temperature distributions, and white lines represent isotherms. We can observe that the isotherms in the matrix are straight lines, indicating that the temperature distribution in the matrix is not affected by the structure. At the same time, the isotherms in the core are denser than those in the matrix, which indicates that the structure plays the role of thermal concentrating.

Figure 4(b) shows thermal cloaking at high temperatures. The parameters of the bilayer structure and matrix are the same as those in fig. 4(a). The left and right sides are set at 1600 K and 1700 K, respectively. It can be seen that the isotherms in the matrix are straight lines. Meanwhile, there is no isotherm in the core, indicating that the core maintains a constant temperature, and thermal cloaking is achieved.

The switchable behavior can be well understood with the following explanation. The designed nonlinear thermal conductivity is composed of a linear term and a nonlinear term. At low temperatures such as 300–400 K, the linear term is dominant, so the device behaves as a concentrator. At high temperatures such as 1600–1700 K, the nonlinear term is dominant, so the device acts as a cloak. Therefore, the performance can be still satisfying at other temperature intervals, as long as only one term (either the linear term or the nonlinear term) is dominant. Theoretically speaking, the device can always maintain a good performance as long as the temperatures do not reach the melting point of the material. For sample fabrications, practical materials like aerogels are good candidates to have a tolerance of high temperatures up to more than 2000 K [49,50], so our design is applicable at high temperatures. Compared with an existing study on thermal cloak-concentrator [36], our design considers the global nonlinearity of the system rather than a local nonlinearity, so the temperature distributions in the matrix are distinctly different. Moreover, our nonlinearity results from thermal radiation, and the nonlinearity in the study [36] relies on shape memory alloys.

Three-dimensional theory. – The present theory can also be extended to three-dimensional cases. Similarly, we consider a core-shell metamaterial embedded in a matrix. The nonlinear thermal conductivities of the core $\kappa_c'(T)$, shell $\kappa_s'(T)$, and matrix $\kappa_m'(T)$ are denoted as

$$\kappa_c'(T) = \sum_{i=1}^{n} \alpha_i' T^{\lambda_i'}, \tag{22}$$

$$\kappa_s'(T) = \sum_{i=1}^{n} \beta_i' T^{\lambda_i'}, \tag{23}$$

$$\kappa'_m(T) = \sum_{i=1}^{n} \gamma'_i T^{\lambda'_i}, \tag{24}$$

where α'_i, β'_i, γ'_i, and λ'_i can be any constants. We also suppose that $\kappa'_s(T)/\kappa'_c(T) = \mu'$ and $\kappa'_m(T)/\kappa'_c(T) = \nu'$, where μ' and ν' are two constants. Therefore, the dominant equation in the core can be expressed as

$$\boldsymbol{\nabla} \cdot [-\kappa'_c(T)\boldsymbol{\nabla} T] = \boldsymbol{\nabla} \cdot \left[-\sum_{i=1}^{n} \alpha'_i T^{\lambda'_i} \boldsymbol{\nabla} T \right] = 0. \tag{25}$$

By setting $\alpha'_j/\alpha'_i = \omega'_j$, we can obtain

$$\boldsymbol{\nabla} \cdot \left[-\alpha'_i \boldsymbol{\nabla} \left(\sum_{j=1}^{n} \frac{\omega'_j}{\lambda'_j + 1} T^{\lambda'_j + 1} \right) \right] = 0. \tag{26}$$

With $\beta'_i/\alpha'_i = \mu'$, $\gamma'_i/\alpha'_i = \nu'$, and $\alpha'_j/\alpha'_i = \omega'_j$, we can also derive $\beta'_j/\beta'_i = \omega'_j$ and $\gamma'_j/\gamma'_i = \omega'_j$, so the dominant equation in the shell and matrix can be expressed as

$$\boldsymbol{\nabla} \cdot \left[-\beta'_i \boldsymbol{\nabla} \left(\sum_{j=1}^{n} \frac{\omega'_j}{\lambda'_j + 1} T^{\lambda'_j + 1} \right) \right] = 0, \tag{27}$$

$$\boldsymbol{\nabla} \cdot \left[-\gamma'_i \boldsymbol{\nabla} \left(\sum_{j=1}^{n} \frac{\omega'_j}{\lambda'_j + 1} T^{\lambda'_j + 1} \right) \right] = 0. \tag{28}$$

We make a substitution

$$\varphi' = \sum_{j=1}^{n} \frac{\omega'_j}{\lambda'_j + 1} T^{\lambda'_j + 1}, \tag{29}$$

so eqs. (5)–(7) can be expressed in spherical coordinates (r, θ, ϕ) as

$$\frac{\partial}{\partial r}\left(r^2 \frac{\partial \varphi'}{\partial r} \right) + \frac{1}{\sin\theta} \frac{\partial}{\partial \theta}\left(\sin\theta \frac{\partial \varphi'}{\partial \theta} \right) = 0, \tag{30}$$

where ϕ vanishes because we consider the spherically symmetric case. Equation (30) is a linear equation, so its general solution is [45]

$$\varphi' = \sum_{l=0}^{\infty} [A_l r^l + B_l r^{-(l+1)}] P_l(\cos\theta). \tag{31}$$

With the boundary conditions similar to eq. (12), we can know $\varphi'_c = A'_{c1} r \cos\theta$, $\varphi'_s = (A'_{s1} r + B'_{s1} r^{-2}) \cos\theta$, and $\varphi'_m = (A'_{m1} r + B'_{m1} r^{-2}) \cos\theta$. Therefore, by solving eq. (12) with $B'_{m1} = 0$, we can obtain

$$\gamma'_i = \beta'_i \frac{\alpha'_i + 2\beta'_i + 2(\alpha'_i - \beta'_i)p'}{\alpha'_i + 2\beta'_i - (\alpha'_i - \beta'_i)p'}, \tag{32}$$

where $p' = r_c'^3/r_s'^3$ is core fraction. Since we do not restrict the value of i, it can take values from 1 to n. Therefore, the nonlinear thermal conductivity of the matrix (namely the effective thermal conductivity of the core-shell metamaterial) should satisfy

$$\kappa'_m(T) = \sum_{i=1}^{n} \beta'_i \frac{\alpha'_i + 2\beta'_i + 2(\alpha'_i - \beta'_i)p'}{\alpha'_i + 2\beta'_i - (\alpha'_i - \beta'_i)p'} T^{\lambda'_i}. \tag{33}$$

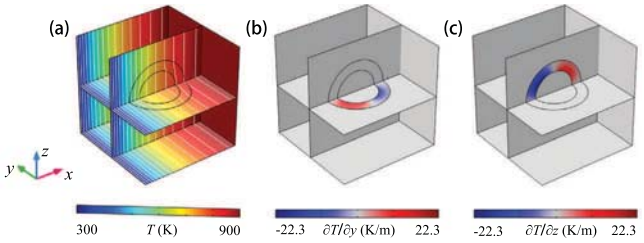

Fig. 5: Three-dimensional simulations of a rigorous case. The simulation size is $8 \times 8 \times 8$ m^3, $r'_c = 2$ m, and $r'_s = 3$ m ($p' = 0.296$). The thermal conductivities of the core, shell, and matrix are $10^2 + 10^{-2}T + 10^{-4}T^2 + 10^{-6}T^3$ W/(m · K), $50 + 5 \times 10^{-3}T + 5 \times 10^{-5}T^2 + 5 \times 10^{-7}T^3$ W/(m · K), and $62 + 6.2 \times 10^{-3}T + 6.2 \times 10^{-5}T^2 + 6.2 \times 10^{-7}T^3$ W/(m · K), respectively. (a) Temperature distribution. (b) $\partial T/\partial y$ distribution. (c) $\partial T/\partial z$ distribution.

We also perform a finite-element simulation to test the three-dimensional theory, and obtain the temperature distribution of the system (see fig. 5(a)). The isotherms in the matrix are straight lines and parallel to the z-axis, indicating that the the thermal conductivity of the matrix is equal to the effective thermal conductivity of the core-shell metamaterial. We also plot the $\partial T/\partial y$ and $\partial T/\partial z$ distributions in the matrix (see figs. 5(b) and (c), respectively). According to our theory, these two values in the matrix are 0, which is also confirmed by the simulations.

Discussion and conclusion. – The present theory is rigorous in both two and three dimensions as long as the ratio of the nonlinear thermal conductivities of the core and shell is a constant. If the ratio is not a constant, the present theory is approximate but still applicable. Certainly, the scheme can be extended to elliptical/ellipsoidal cases [9,43]. Meanwhile, the scheme can also be extended to deal with transient cases as long as we take density and heat capacity into consideration [9,43].

To sum up, we have proposed a rigorous theory to calculate the effective thermal conductivities of core-shell metamaterials with nonlinear thermal conductivities, whether weak or strong. For intelligent applications, we further design a bilayer metamaterial with switchable functions between thermal concentrating at low temperatures and thermal cloaking at high temperatures. The feasibility of this method is also confirmed by finite-element simulations. These results may also have potential applications for heat transfer at microscopic scale where nonlinearity is common [51,52], such as realizing thermal camouflage [53,54].

* * *

We acknowledge the financial support by the National Natural Science Foundation of China under Grant No. 11725521.

REFERENCES

[1] Fan C. Z., Gao Y. and Huang J. P., *Appl. Phys. Lett.*, **92** (2008) 251907.
[2] Chen T. Y., Weng C. N. and Chen J. S., *Appl. Phys. Lett.*, **93** (2008) 114103.
[3] Narayana S. and Sato Y., *Phys. Rev. Lett.*, **108** (2012) 214303.
[4] Xu H. Y., Shi X. H., Gao F., Sun H. D. and Zhang B. L., *Phys. Rev. Lett.*, **112** (2014) 054301.
[5] Han T. C., Bai X., Gao D. L., Thong J. T. L., Li B. W. and Qiu C. W., *Phys. Rev. Lett.*, **112** (2014) 054302.
[6] Ma Y. G., Liu Y. C., Raza M., Wang Y. D. and He S. L., *Phys. Rev. Lett.*, **113** (2014) 205501.
[7] Han T. C., Bai X., Thong J. T. L., Li B. W. and Qiu C. W., *Adv. Mater.*, **26** (2014) 1731.
[8] Chen T. Y., Weng C. N. and Tsai Y. L., *J. Appl. Phys.*, **117** (2015) 054904.
[9] Han T. C., Yang P., Li Y., Lei D. Y., Li B. W., Hippalgaonkar K. and Qiu C. W., *Adv. Mater.*, **117** (2018) 1804019.
[10] Li Y., Zhu K. J., Peng Y. G., Li W., Yang T. Z., Xu H. X., Chen H., Zhu X. F., Fan S. H. and Qiu C. W., *Nat. Mater.*, **18** (2019) 48.
[11] Zhou L. L., Huang S. Y., Wang M., Hu R. and Luo X. B., *Phys. Lett. A*, **383** (2019) 759.
[12] Li J. X., Li Y., Li T. L., Wang W. Y., Li L. Q. and Qiu C. W., *Phys. Rev. Appl.*, **11** (2019) 044021.
[13] Kapadia R. S. and Bandaru P. R., *Appl. Phys. Lett.*, **105** (2014) 233903.
[14] Xu G. Q., Zhou X. and Zhang J. Y., *Int. J. Heat Mass Transfer*, **142** (2019) 118434.
[15] He X. and Wu L. Z., *Phys. Rev. E*, **88** (2013) 033201.
[16] Yang T. Z., Bai X., Gao D. L., Wu L. Z., Li B. W., Thong J. T. L. and Qiu C. W., *Adv. Mater.*, **27** (2015) 7752.
[17] Yang T. Z., Su Y. S., Xu W. K. and Yang X. D., *Appl. Phys. Lett.*, **109** (2016) 121905.
[18] Hou Q. W., Zhao X. P., Meng T. and Liu C. L., *Appl. Phys. Lett.*, **109** (2016) 103506.
[19] Li Y., Bai X., Yang T. Z., Luo H. and Qiu C. W., *Nat. Commun.*, **9** (2018) 273.
[20] Hu R., Zhou S. L., Li Y., Lei D. Y., Luo X. B. and Qiu C. W., *Adv. Mater.*, **30** (2018) 1707237.
[21] Zhou S. L., Hu R. and Luo X. B., *Int. J. Heat Mass Transfer*, **127** (2018) 607.
[22] Hu R., Huang S. Y., Wang M., Luo X. L., Shiomi J. and Qiu C. W., *Adv. Mater.*, **31** (2019) 1807849.
[23] Xu L. J., Yang S. and Huang J. P., *Phys. Rev. Appl.*, **11** (2019) 034056.
[24] Peng X. Y. and Hu R., *ES Energy Environ.*, **6** (2019) 39.
[25] Yang F. B., Xu L. J. and Huang J. P., *ES Energy Environ.*, **6** (2019) 45.
[26] Yang S., Xu L. J. and Huang J. P., *EPL*, **126** (2019) 54001.
[27] Xu L. J., Yang S. and Huang J. P., *Eur. Phys. J. B*, **92** (2019) 264.
[28] Xu L. J., Yang S. and Huang J. P., *Phys. Rev. Appl.*, **11** (2019) 054071.
[29] Yang S., Xu L. J. and Huang J. P., *EPL*, **128** (2019) 34002.
[30] Xu L. J. and Huang J. P., *Sci. China-Phys. Mech. Astron.*, **63** (2020) 228711.
[31] Li Y., Shen X. Y., Wu Z. H., Huang J. Y., Chen Y. X., Ni Y. S. and Huang J. P., *Phys. Rev. Lett.*, **115** (2015) 195503.
[32] Huang S. Y., Zhang J. W., Wang M., Lan W., Hu R. and Luo X. B., *ES Energy Environ.*, **6** (2019) 51.
[33] Dai G. L., Shang J., Wang R. Z. and Huang J. P., *Eur. Phys. J. B*, **91** (2018) 59.
[34] Dai G. L. and Huang J. P., *Int. J. Heat Mass Transfer*, **147** (2019) 118917.
[35] Yang S., Xu L. J. and Huang J. P., *Phys. Rev. E*, **99** (2019) 042144.
[36] Shen X. Y., Li Y., Jiang C. R., Ni Y. S. and Huang J. P., *Appl. Phys. Lett.*, **109** (2016) 031907.
[37] Ming Y., Li H. M. and Ding Z. J., *Phys. Rev. E*, **93** (2016) 032127.
[38] Nguyen K. L., Merchiers O. and Chapuis P. O., *Appl. Phys. Lett.*, **112** (2018) 111906.
[39] Yang Y., Chen H. Y., Wang H., Li N. B. and Zhang L. F., *Phys. Rev. E*, **98** (2018) 042131.
[40] Kang S., Cha J., Seo K., Kim S., Cha Y., Lee H., Park J. and Choi W., *Int. J. Heat Mass Transfer*, **130** (2019) 469.
[41] Zhou Z. Y., Shen X. Y., Fang C. C. and Huang J. P., *ES Energy Environ.*, **6** (2019) 85.
[42] Wang J., Dai G. L., Yang F. B. and Huang J. P., *Phys. Rev. E*, **101** (2020) 022119.
[43] Xu L. J. and Huang J. P., *Phys. Rev. Appl.*, **12** (2019) 044048.
[44] Xu L. J., Dai G. L. and Huang J. P., *Phys. Rev. Appl.*, **13** (2020) 024063.
[45] Xu L. J., Yang S. and Huang J. P., *Phys. Rev. E*, **99** (2019) 022107.
[46] `http://www.comsol.com/`.
[47] Zeller R. C. and Pohl R. O., *Phys. Rev. B*, **4** (1971) 2029.
[48] Glassbrenner C. J. and Slack G. A., *Phys. Rev.*, **134** (1964) A1058.
[49] Hanzawa Y., Hatori H., Yoshizawa N. and Yamada Y., *Carbon*, **40** (2002) 575.
[50] Xu X., Zhang Q. Q., Hao M. L., Hu Y., Lin Z. Y., Peng L. L., Wang T., Ren X. X., Wang C., Zhao Z. P., Wan C. Z., Fei H. L., Wang L., Zhu J., Sun H. T., Chen W. L., Du T., Deng B. W., Cheng G. J., Shakir I., Dames C., Fisher T. S., Zhang X., Li H., Huang Y. and Duan X. F., *Science*, **363** (2019) 723.
[51] Li N. B., Ren J., Wang L., Zhang G., Hanggi P. and Li B. W., *Rev. Mod. Phys.*, **84** (2012) 1045.
[52] Bao H., Chen J., Gu X. K. and Cao B. Y., *ES Energy Environ.*, **1** (2018) 16.
[53] Liu Y. D., Cheng Y. H., Hu R. and Luo X. B., *Phys. Lett. A*, **383** (2019) 2296.
[54] Hu R. and Luo X. B., *Natl. Sci. Rev.*, **6** (2019) 1071.